WWLLN lightning and satellite microwave radiometrics at 37 to 183 GHz: Implications for convection and thundercloud charging in the broad tropics

N. N. Solorzano[1,2,3], J. N. Thomas[1,2,4], J. A. Weinman[1*], W. Keane[2,4], M. L. Hutchins[1] and R. H. Holzworth[1]

[1]*Dept. of Earth and Space Sciences, University of Washington, Seattle, WA*

[2]*Northwest Research Associates, Redmond, WA*

[3]*Dept. of Physics, Digipen Institute of Technology, Redmond, WA*

[4]*Dept. of Electrical and Computer Engineering, Digipen Institute of Technology, Redmond, WA*

[*]Deceased

This work is dedicated to the late James (Jim) Weinman, a pioneer in radiative transfer studies and lightning applications in atmospheric physics.

Manuscript submitted to JGR-Atmospheres, August 2012

Abstract

We investigate global atmospheric convection and thundercloud charging mechanisms using data from the World Wide Lightning Location Network (WWLLN) and passive microwave radiometer observations. The radiometric database is provided by the Tropical Rainfall Measuring Mission satellite (TRMM) Microwave Imager (TMI), and the Special Sensor Microwave Imager/Sounder (SSMIS) on the Defense Meteorological Satellite Program (DMSP) satellite F16. Radiometric frequency channels range from 37 to 183 GHz, allowing observations related to several types of precipitating hydrometeors and vertical updrafts. For the first time, measurements from a land-based lightning network are compared with satellite microwave radiometric signatures from multiple platforms on a global scale, thus expanding and complementing the capabilities of previous lightning/radiometer studies. WWLLN lightning rates and minimum radiometer brightness temperatures (BTs) are compared for two northern and southern hemisphere summers (2009-2011) for the broad tropics. We find that: 1) the probabilities of cold BTs, therefore frozen hydrometeors, increase about tenfold in lightning producing clouds compared with non-lightning producing ones, and 2) BTs decrease with increasing lightning rates for all frequency channels examined. These findings are generally independent of land, coast, and ocean regimes. However, the highest probabilities of cold BTs for non-lightning producing clouds are found over the ocean. The results generally support the noninductive thundercloud charging mechanism for the tropics and subtropics. Moreover, WWLLN provides a similar picture of global convection related to BTs as satellite lightning sensors. Thus, WWLLN, or other similar global lightning networks, can potentially be used to fill gaps in satellite lightning and microwave radiometer data.

1. Introduction

The present investigation uses two years of data from the World Wide Lightning Location Network (WWLLN), a ground-based, global network that continually measures lightning discharges, and a dataset of passive microwave radiometer observations at 37 to 183 GHz from two satellite platforms. The Tropical Rainfall Measuring Mission (TRMM) Microwave Imager (TMI) provides brightness temperature (BT) radiances at 37 and 85 GHz, and the Special Sensor Microwave Imager/Sounder (SSMIS) on Defense Meteorological Satellite Program (DMSP) satellite F16 provides radiances at 91, 150 and 183 GHz. The goals of this analysis are to: (1) describe global convection in terms of lightning rate and microwave radiometer data, and (2) study the fundamental relationships between lightning and cloud hydrometeor characteristics on a global scale, particularly ocean/land contrasts.

There are tight relationships between lightning, convection, and cloud hydrometeor distribution and mass [e.g., Toracinta et al., 2002]. High concentrations of hydrometeors can be identified by increased radar reflectivity and decreased passive microwave BTs in the mixed phase region of a thundercloud (located around 0°C to -40°C) [e.g., Cecil and Zipser, 2002]. Numerous investigations have found high correlations between lightning flash rate and precipitation-sized ice mass or ice mass-related parameters, such as ice water path [e.g., Cecil and Zipser, 2002; Petersen et al., 2005; Latham et al., 2007; Deierling and Petersen, 2008; Pessi and Businger, 2009]. Moreover, lightning rates are well correlated with updraft velocities above a threshold of approximately 5 m/s in the mixed-phase environment [e.g, Deierling and Petersen, 2008].

Lightning rates have also been compared with BTs derived from passive microwave channels, especially the ice-scattering signatures. BTs at 37 to 183 GHz are depressed via scattering of upwelling radiation by liquid and frozen cloud hydrometeors [e.g., Wu and Weinman, 1984]. Each frequency has different scattering properties, with higher frequencies more sensitive to smaller particles than lower frequencies. Moreover, the higher frequency channels are more sensitive to emissions by liquid water than the lower

frequency channels [Bennartz and Bauer, 2003], and although supercooled water in the mixed-phase environment is required for charge separation [e.g., Takahashi, 1984], some studies suggest that supercooled water emissions increase the BTs in the 37 -150 GHz range, masking the scattering signal from graupel at the same level. However, this effect has not been quantified [e.g., Cecil and Zipser, 2002]. Commonly used frequency channels reported in past studies are 37 GHz [e.g., Zipser et al., 2006; Liu et al., 2011], 85 - 91 GHz [Toracinta and Zipser, 2001; Boccippio et al., 2000; Nesbitt et al., 2000; Zipser et al., 2006; Cecil et al., 2002; Cecil et al., 2005; Kodama et al., 2007; Nakamura et al., 2011; Liu et al., 2011], 150 - 157 GHz [Hong and Heygster, 2008; Nakamura et al., 2011], all of which are modulated by the ice layer. Other important channels, but not as commonly used, are the water vapor frequencies 183 ± 1, 3 and 7 GHz, which are intense convection trackers [e.g., Hong and Heygster, 2008].

Strong correlations between lightning and cloud ice-related parameters indicate that the noninductive mechanism plays a major role in cloud electrification, dominating the electric field growth and subsequent lightning production in all seasons, on a global scale, for oceanic and land-based thunderstorms [e.g., Latham et al., 2007]. This mechanism involves ice-ice collisional charging, is independent of external electric fields [e.g. Jayaratne et al., 1983; Takahashi, 1984], and relies on vigorous updrafts in the mixed phase region [e.g., Reynolds et al., 1957; Lang and Rutledge, 2002; Wiens et al., 2005; Deierling and Petersen, 2008]. The inductive mechanism, another mean of cloud charging, is described as a non-dominant process that, similarly to the noninductive mechanism, depends on hydrometeor collisions but requires external electric fields [e.g., Mansell et al., 2005]. Inductive charging might play a significant role in the final stages of field-growth, but the efficacy of this mechanism is reduced as the ice content increases in the mixed phase region [e.g., Petersen et al., 2005; Latham et al., 2007]. Conversely, the noninductive mechanism relies on ice production rate. Thus, positive correlations between lightning rates and cloud ice concentration, and therefore BT depressions, support the noninductive mechanism rather than the inductive mechanism.

In the present analysis, intense convection and mixed phase cloud electrification in the tropics and subtropics are investigated by comparing continuous lightning measurements with microwave radiometer data from two satellite platforms. This includes probing the noninductive vs. inductive thundercloud electrification mechanisms on a global scale for land, coast, and ocean regimes. With the exception of Nakamura et al. [2011], who compared WWLLN data to AMSU-B radiometrics, all previous global lightning/radiometer studies used satellite lightning observations from the Lightning Imager Sensor (LIS) on TRMM or the Optical Transient Detector (OTD). Here, for the first time, lightning from a global, land-based network (WWLLN) is compared with microwave data from multiple satellite platforms.

2. Data and Methods

The WWLLN (currently 60 stations worldwide, http://wwlln.net) provides real-time lightning locations globally by measuring the Time Of Group Arrival (TOGA) of Very Low Frequency (VLF) electromagnetic radiation (3-30 kHz) generated by lightning discharges [Dowden et al., 2002; Rodger et al., 2006]. The location accuracy and efficiency of WWLLN have been determined for certain regions of the globe by comparison to regional, ground-based, lightning detection systems [Lay et al., 2004; Rodger et al., 2005, 2006, 2009; Jacobson et al., 2006; Abarca et al., 2010; Hutchins et al., 2012a]. Rodger et al. [2009] used a comparison between WWLLN and the New Zealand Lightning Detection Network (NZLDN) and Monte Carlo simulation techniques to estimate the global location accuracy of WWLLN, and Abarca et al. [2010] conducted a performance assessment of WWLLN using the National Lightning Detection Network (NLDN) as ground-truth over the contiguous US. In these studies, the overall detection efficiency of cloud-to-ground (CG) flashes increased from about 4% in 2006-2007 to about 11% in 2008-2009 (>30% for strokes with peak currents > 35 kA), and location and timing errors were less than 10 km and 10 microseconds, respectively. In a comparison of WWLLN with the Earth Networks Total Lightning Network (ENTLN) for 2011 over the continental US, Hutchins et al. [2012a] found that the WWLLN detection efficiency was about 16% for CG strokes, 2% for in-cloud (IC) lightning, and 5% overall. The mean location accuracy was about 5 km, and for CG strokes above 20 kA the detection

efficiency increased to 38%. Approximately 64% of WWLLN-ENTLN matched lightning were CG strokes, whereas 19% of all ENTLN detected lightning were CG strokes. Thus WWLLN detects both CG and IC lightning, but since it is biased towards lightning that radiate strongly in the VLF, it detects CG strokes more efficiently than IC lightning.

Quantifying the detection efficiency of WWLLN is important for comparing lightning with radiometer data. Hutchins et al. [2012b] developed a technique to generate near real-time, global relative detection efficiency (DE) maps for WWLLN with a temporal resolution of 1-hr and spatial resolution of 1°×1°. The relative DE corrections account for changes in the ionosphere and the operational status of stations, and thus provide uniform global detection efficiency. Relative DE corrections can be applied to all archived WWLLN data recorded since Apr. 2009, and we use only relative DE corrected data in our analysis.

The radiometric database used in this study combines TMI and SSMIS/F16 measurements of BTs. These are Level 1C data from Colorado State University (http://mrain.atmos.colostate.edu/LEVEL1C/). Table 1 summarizes the characteristics of the TMI and SSMIS microwave channels we use. In addition to these channels, polarization corrected temperatures (PCT), a weighted difference of vertical and horizontal polarizations to minimize surface emissivity effects from land and ocean, are found for TMI 37 and 85 GHz, and SSMIS 91 GHz channels [e.g., Nesbitt and Zipser, 2003]. TMI and SSMIS have some notable similarities and differences. Firstly, both have conical scan geometries that provide uniform spatial resolution, polarization purity, and common concentric fields for all instrument channels across their swaths [Kummerow et al., 1998; Yan and Weng, 2009]. Moreover, both instruments are on low-earth orbiting (LEO) satellites allowing a particular region of Earth to be observed for only a few minutes each day. Although both are on LEO satellites, their actual orbits are quite different. The polar-orbiting DMSP satellites are in circular sun-synchronous low orbits (830 km altitude), and they cross the equator at the same local solar time (LST) twice each day, once ascending (N to S) and once descending. Specifically, during the years studied here (2009-2011), DMSP/F16 crossed the equator at about 19:00

LST ascending and 07:00 LST descending with a period of 101 minutes (~14 orbits daily) (orbit degradation causes slow changes in these values over time; see http://www.ssmi.com/support/crossing_times.html). In contrast, the TRMM orbit is circular, non-sun-synchronous, and at an inclination of 35° (~400 km altitude) with a period of about 90 minutes (~16 orbits daily) that allows it to observe surface locations at different daily local times and provide extensive coverage of the tropics. The main implication of these orbital differences is that SSMIS/F16 tends to observe thunderstorms that occur at about 19:00 and 07:00 LST, whereas TMI observes thunderstorms at various LSTs.

The TMI and SSMIS/F16 radiometers provide BTs with resolutions and swath widths as indicated in Table 1. We parse these data by taking the minimum BTs in 0.5° × 0.5° mapping-bins for the TMI and SSMIS/F16 frequency channels listed in Table 1, and the corresponding calculated PCTs. WWLLN data are parsed in the same 0.5° × 0.5° mapping-bins by counting the number of DE-corrected lightning within ± 15 min. of the BT measurements. Hence only WWLLN lightning coincident with BTs are considered. We thus define a data *sample* as one ± 15 min. lightning count and the minimum BTs for all channels and corresponding PCTs for each 0.5° × 0.5° mapping-bin scanned by TMI or SSMIS/F16. Mapping-binned data for two northern and southern hemisphere summers are combined into a summer database, namely Jul., Aug., and Sep. (JAS) of 2009 and 2010 for 0°-35° N and Jan., Feb., and Mar. (JFM) of 2010 and 2011 for 0°-35° S. These mapping-binned data are then organized into ocean, coast, and land domains using 0.5° × 0.5° resolution, and lightning rates are converted into units of $1/km^2/day$. In total, this analysis includes more than 7 million relative DE corrected WWLLN lightning events coincident with satellite radiometer observations from TMI and SSMIS/F16.

Data presented in Figures 1, 2, and 3 require some additional processing using the mapping-binned data described above as input. Namely, Figure 1 a and c display the probabilities of BTs below a given threshold and require at least five samples per 0.5° × 0.5° mapping-bin, where each sample must have a

minimum of two lightning counts (or 0.016 lightning 1/km^2/day). Figures 2 and 3 are scatter plots that present mapping-binned data redistributed by lightning rate in lightning-bins with a width of five lightning per ± 15 min. per 0.5° × 0.5° (or 0.08 lightning 1/km^2/day). To remove statistical outliers, only lightning-bins with at least five samples are included. Circles represent the average of minimum BTs within a lightning-bin and the error bars are the standard deviations of the BTs.

3. Results and Discussion

Figure 1 presents a time-integrated, panoramic view of the broad tropics (35° S to 35° N) from two ice-scattering signatures, TMI 85 GHz PCT and SSMIS/F16 150 GHz H. The maps show the probabilities of cold BTs with and without lightning for the warm seasons of 2009-2010 in the Northern Hemisphere (JAS), and 2010-2011 in Southern Hemisphere (JFM). Figures 1a and c display the probabilities (in percent) of BTs below a threshold for TMI 85 GHz PCT and SSMIS 150 GHz H, respectively, for at least five samples per mapping-bin, where each sample must have a minimum of two lightning counts. The two-lightning count criterion is chosen to exclude mapping-bins with a single WWLLN DE corrected lightning event, which helps to assure that only active thundercloud cells are selected. The BT threshold for TMI 85 GHz PCT is 195 K, while the threshold for SSMIS 150 GHz H is 180 K. These criteria are based on the population of BTs in terms of lightning rate as displayed in Figures 2b and 3b. As in Figures 1a and c, Figures 1b and d also contain the probabilities of BTs. However, here the probabilities are conditioned to zero lightning in each 0.5° × 0.5° mapping-bin. The TMI 85 GHz PCT channel is one of the most commonly used frequencies for comparisons between an ice-modulated channel and lightning, and the SSMIS 150 GHz H results, also frequently used in such comparisons, are displayed here for comparative purposes.

In general, the main convection regions shown in Figures 1a and c agree with the description by Mohr et al. [1999] as the areas where the majority of the tropical rainfall and the mesoscale convective systems occur, and by Boccippio et al. [2000] in terms of regional variability in the lightning distribution (see

Figure 1 in Mohr et al. [1999] and Figure 1 in Boccippio et al. [2000]). They used a database of precipitating cloud clusters from 85 GHz data for three consecutive months during each region's wet seasons and found significant differences between their BT spectra. The present work confirms these areas as highly convective in the summer. Importantly, although there is good qualitative agreement between Figures 1a and c and Boccippio et al. [2000], the scope of this report is a global analysis. Detailed regional analyzes using WWLLN and microwave data are the focus of ongoing studies. Note that data are parsed using different months for each hemisphere (JAS for Northern Hemisphere and JFM for Southern Hemisphere), causing the apparent BT discontinuity around the equator. Overall, Figures 1a and c also qualitatively agree with Figure 1 of Petersen et al. [2005] (for example), who used LIS lightning and ice water path (instead of BTs) for summer months.

According to Bennartz and Bauer [2003], the response of microwave BTs to ice scattering markedly increases with frequency and the 150 GHz channel is 2 – 2.5 times more sensitive to cloud water emissions than 85 GHz. Thus, the probabilities of cold BTs in Figure 1 are related mostly to ice and water scattering in clouds, possibly with a warming effect from supercooled water. The 85 GHz PCT and 150 GHz probabilities are generally very similar for much of the globe. But there are some differences that are likely attributed to the contrasting sensitivities to cloud hydrometeors, such as the presence of higher probabilities of colder BTs at 150 GHz H in the Sub-Saharan region in Figure 1c. Bennartz and Bauer [2003] also found that the 85 GHz H/V channels are more affected by surface emissivity, but in Figure 1 85 GHz PCT rather than V or H is presented, hence most of the surface effects are minimized. However, ice and snow coverage in the Andes and Himalayan Mountain regions (for example) are likely causing anomalously low probabilities in Figure 1a and c and high probabilities in Figure 1b.

Figures 1b and d display the probabilities of BTs conditioned to zero lightning. Note that there is an order-of-magnitude difference in the results with and without lightning, and that there are different color scales for 85 and 150 GHz. While, in the presence of lightning, the typical probability of BTs below the

thresholds for each channel is 50%, the probability of cold BTs in the absence of lightning is usually below 5% for both channels. Through the contrasts in BT probabilities with and without lightning, it is possible to see that, generally, if there is lightning present, then the BTs are colder. In other words, lightning is associated with larger masses of frozen hydrometeors. These contrasts would be expected in the context of both the inductive and noninductive mechanisms of cloud electrification, as both involve collisions between hydrometeors. Figure 1 does not provide evidence that one mechanism would prevail, since the noninductive mechanism can only be probed by comparing the lightning rate with BTs (therefore mass of frozen hydrometeors). This relationship is presented in Figures 2, 3 and 4.

An interesting feature of Figures 1a – d is the oceanic probabilities of BTs. Figures 1a and c indicate that the probabilities of cold BTs associated with lightning over the oceans are often high. Moreover, Figures 1b and d show that the probabilities of cold BTs that are independent of lightning occurrence are higher over the oceans when compared to the land, especially around the equator. These results add to the findings of Xu and Zipser [2012], who pointed out that mixed-phase processes dominate continental convection, while only about 10% of the oceanic convection involves such processes. The noninductive mechanism requires the presence of supercooled water and vigorous updrafts in addition to frozen hydrometeors in the mixed phase region [Latham et al., 2007]. Thus, depressed BTs alone, which do not quantify supercooled water, are not indicators for cloud electrification over the ocean.

To probe noninductive vs. inductive charging, scatter plots of average minimum BTs vs. lightning rates for land (green), coast (red), and ocean (blue) regimes are shown in Figures 2 (TMI) and 3 (SSMIS/F16). Circles represent the average of minimum BTs using a lightning-bin width of five lightning per ± 15 min. per mapping-bin° (or 0.08 lightning 1/km^2/day), and the error bars are the standard deviations of the BTs. Outliers are removed by requiring at least five samples per lightning-bin. As described in Section 2, the lightning-bins used to find the averages and standard deviations in Figure 2 and 3 are distinct from the 0.5° × 0.5° mapping-bins used to initially parse the data. Cubic least-squares fits to the average BTs (solid

261 lines connecting the circles) are shown, along with the total number of lightning used and removed in
262 each regime. The cumulative distribution functions (CDFs) of the lightning rate samples for each channel
263 are presented on the right ordinates.
264
265 Figures 2 and 3 convey that increased lightning activity is associated with decreased BTs (hence
266 increased frozen hydrometeor population) for all the channels, indicating that the noninductive
267 mechanism plays a significant role in land, coast, and ocean regimes. Although a cubic fit is chosen, the
268 standard deviations are large, and thus this kind of relationship can be approximately linear, such as, for
269 example, the results found by Petersen et al. [2005], or cubic, as proposed by Nakamura et al. [2011]. The
270 only notable differences between regimes are seen at high lightning rates, where the negative trends of
271 ocean regime curves are much weaker than land and coastal trends. This could be indicative of less
272 dependence on the noninductive mechanism at high lightning rates over the ocean, but this is only
273 speculative because the number of samples at high lightning rates is low.
274
275 Figure 2a presents TMI 37 GHz PCT versus lightning rates, presenting a markedly weaker trend
276 (compared to the other channels) between minimum BTs and lightning. This is due to the reduced
277 response of this channel to ice particles as reported by Bennartz and Bauer [2003] (for example). Figure
278 2b (TMI 85 GHz PCT) shows a strong relationship between frozen hydrometeors and lightning counts. In
279 comparing Figures 2b (TMI 85 GHz PCT) and 3a (SSMIS 91 GHz PCT), the cubic fit curve is steeper for
280 the 85 GHz channel. This could be the result of inherent, nonlinear physical differences between 85 and
281 91 GHz ice scattering, such as reported by Hawkins et al. [2008], who compared SSMIS 91 GHz and
282 Special Sensor Microwave/Imager (SSM/I) 85 GHz channels. Differences between the TMI and SSMIS
283 sensors and platforms could also play a role. TMI 85 GHz has higher resolution than SSMIS 91 GHz (see
284 Table 1), and TRMM observes storms at various local solar times (LSTs) while DMSP/F16 observes at
285 fixed LSTs. And it should be noted that TRMM and SSMIS have not been cross-calibrated at these
286 frequencies. For the three SSMIS water vapor channels (183.3 ± 1, ±3, ±7 GHz), two of which are shown

Figure 3, the BT depressions increase with channel width (183.3 ±3 GHz is not shown in Figure 3 but is intermediate in slope to 183.3 ± 1 and ±7 GHz). Moreover, the relationships between BTs and lightning in Figures 3b (SSMIS 150 GHz H) and 3d (SSMIS 183 ± 7 GHz H) are remarkably similar. This is because the 183.3 ± 7 GHz channel can view deeper into clouds than the other two water vapor channels [Burns et al., 1997; Hong et al., 2005], and, like the 150 GHz channel, is highly sensitive to frozen hydrometeors. These similar behaviors show that these two SSMIS channels deliver similar responses to intense convection.

The cumulative distribution functions (CDFs) on the right ordinates of Figure 2 and 3 give the proportion (in percent) of the lightning rate sample population less than or equal to the lightning rate value on the abscissa. Steeper CDF slopes correspond to distributions with a higher percentage of lower lightning rates. The CDFs in Figures 2 and 3 present a different behavior than observed by Petersen et al. [2005], who found that the land regime was associated with a less steep CDF increase (compared with the ocean and the coast) and higher lightning rate sample population for higher ice water path values. Conversely, Figures 2 and 3 show that steeper CDFs are associated to the land regime. It is speculated that this difference can be explained by the types of lightning that WWLLN detects, since WWLLN is biased towards lightning that radiate strongly in the VLF, but it could also be due to different processing techniques employed by Petersen et al. to remover outliers.

Figure 4 shows scatter plots of (a) TMI 37 vs. 85 GHz PCT and (b) SSMIS 91 GHz PCT vs. 150 GHz H with coincident mean lightning rates for land, coast, ocean and all three regimes integrated. The objective here is to probe the noninductive mechanism by using dual-frequency space. Because the presence of ice particles noticeably depresses BTs at 37 and 85 GHz [e.g., Wu and Weinman, 1984], examining lightning coincidence with dual-channels such as 37 and 85 GHz corresponds to comparing lightning activity with a vertically-integrated ice water path weighted towards the larger frozen hydrometeors, although the presence of cloud water prevents the complete vertical characterization of the ice mass [e.g.,

Vivekanandan et al., 1991; Cecil et al., 2005]. Unlike in Figures 2 and 3, no data are excluded from these plots, allowing the full picture of lightning rates to be presented with dual frequencies. As in Figures 2 and 3, warmer BTs are related to decreased lightning rates, and the highest lightning rates are mostly at the coldest BTs, a result that is especially evident for the oceanic and coastal regimes. In agreement with reports such as Cecil et al. [2005] and Nakamura et al. [2011], high lightning rates favor the right side of the population (towards higher 85 GHz PCT or 150 GHz H BTs). Cecil et al. [2005] speculated that this could be due to the transition from Rayleigh scattering to Mie scattering as hydrometeor sizes change, or emissions from supercooled water or rainwater warming the higher frequency (85 and 150 GHz) temperatures and enhancing conditions for cloud electrification. Both explanations have implications for cloud charging mechanisms and will be the focus of future analyses. The results presented in Figure 4 evince a negative, although nonlinear, trend between lightning rates and dual frequency BTs. In the noninductive charging mechanism, lightning rates increase with increasing frozen hydrometeor mass (or BT depressions); thus, the data presented in Figure 4 support the noninductive mechanism and further solidify the results presented in Figures 2 and 3.

4. Conclusions

Lightning from a ground-based, global network and radiometer data from two satellite platforms were compared. For the tropics and subtropics, it is found that the probabilities of cold brightness temperatures (BTs) increase by about one order-of-magnitude in lightning producing clouds compared with non-lightning producing clouds, and BTs decrease with increasing lightning rates for all frequency channels examined. These findings are generally independent of land, coast, and ocean regimes. However, the highest probabilities of cold BTs for non-lightning producing clouds are found over the ocean. The steepness of BTs vs. lightning rate trends depends on the frequency channel employed, with SSMIS 150 and 183 ± 7 GHz H measurements showing nearly identical relationships to lightning. The quantitative results generally support the noninductive thundercloud charging mechanism, and they agree with previous studies that focused mainly on lightning and radiometer data at 37 and 85 GHz from the LIS and

TMI instruments on the TRMM satellite. Ongoing and future analyses include examining seasonal and regional variations of relationships between WWLLN lightning and microwave radiometer data, as well as case studies of storm systems such as mesoscale convective systems and tropical cyclones [Solorzano et al., 2011].

Our results have important implications for future applications of data from VLF lightning networks such as WWLLN. It is shown that these networks can provide a similar picture of global convection related to BTs as satellite lightning sensors such as LIS, even though VLF networks are biased towards strong lightning. Additionally, since low-earth orbiting satellites like TRMM and DMSP/F16 only observe a particular region on Earth for a few minutes daily, VLF networks can potentially be used to fill in these microwave radiometer data gaps. The utilization of lightning data may become even a higher priority in the near future, as the number of space-borne observing instruments of NASA and NOAA may decline to 25% of the current number by 2020 as reported by the National Academy of Sciences/National Research Council Report of May 2012 (https://download.nap.edu/catalog.php?record_id=13405). This study has also helped to quantify lightning as a proxy for deep convection and cloud hydrometeor distributions for future geostationary lightning imagers such as the Geostationary Lightning Mapper (GLM) on the GOES-R/GOES-S satellites scheduled to be launched starting in 2015 (www.goes-r.gov).

Acknowledgments

This research was supported by NSF grant AGS-0947130 and DARPA grant HR011-10-1-0060 to the University of Washington. Partial support was also received from the Digipen Institute of Technology and NorthWest Research Associates. We thank Gad Levy for reading a draft manuscript. The authors wish to thank the World Wide Lightning Location Network (http://wwlln.net), a collaboration among over 50 universities and institutions, for providing the lightning location data used in this report.

References

Abarca, S. F., K. L. Corbosiero, and T. J. Galarneau Jr. (2010), An evaluation of the Worldwide Lightning Location Network (WWLLN) using the National Lightning Detection Network (NLDN) as ground truth, *J. Geophys. Res.*, 115, D18206, doi:10.1029/2009JD013411.

Bennartz, R. and P. Bauer (2003), Sensitivity of microwave radiances at 85–183 GHz to precipitating ice particles, *Radio Sci.*, vol. 38, no. 4, 8075. DOI:10.1029/2002RS002626.

Boccippio, D. J., S. J. Goodman, S. Heckman (2000), Regional Differences in Tropical Lightning Distributions, *J. Appl. Meteor.*, 39, 2231–2248, doi:http://dx.doi.org/10.1175/1520-0450(2001)040<2231:RDITLD>2.0.CO;2

Burns, B. A., X. Wu, and G. R. Diak (1997), Effects of precipitation and cloud ice on brightness temperatures in AMSU moisture channels, *IEEE Trans. Geosci. Remote Sens.*, 35, 1429–1437.

Cecil, D. J., and E. J. Zipser (2002), Reflectivity, ice scattering, and lightning characteristics of hurricane eyewalls and rainbands. Part II: Intercomparison of observations, *Mon. Wea. Rev.*, 130**,** 785–801.

Cecil, D. J., and E. J. Zipser, and S. W. Nesbitt (2002), Reflectivity, ice scattering, and lightning characteristics of hurricane eyewalls and rain- bands. Part I: Quantitative description, *Mon. Wea. Rev.*, 130**,** 769–784.

Cecil, D. J., S. J. Goodman, D. J. Boccippio, E. J. Zipser, and S. W. Nesbitt (2005), Three years of TRMM precipitation features. Part I: Radar, radiometric, and lightning characteristics, *Mon. Wea. Rev.*, 133, 543-566.

391 Deierling, W., and W. A. Petersen (2008), Total lightning activity as an indicator of updraft
392 characteristics, *J. Geophys. Res.*, *113*, D16210, doi:10.1029/2007JD009598.
393
394 Dowden, R. L., J. B. Brundell, and C. J. Rodger (2002), VLF lightning location by time of group arrival
395 (TOGA) at multiple sites, *J. Atmos. Sol. Terr. Phys.*, 64(7), 817–830, doi:10.1016/S1364-6826(02)00085-
396 8.
397
398 Hong, G., G. Heygster, J. Miao, and K. Kunzi (2005), Detection of tropical deep convective clouds from
399 AMSU-B water vapor channels measurements, *J. Geophys. Res.*, 110, D05205,
400 doi:10.1029/2004JD004949.
401
402 Hong. G. and G. Heygster (2008), Intense tropical thunderstorms detected by the Special Sensor
403 Microwave Imager/Sounder, *IEEE Trans. Geosci. Remote Sens.*, 46, no.4, 10.1109/TGRS.2008.915750.
404
405 Hutchins, M. L., R. H. Holzworth, J. B. Brundell, S. Heckman, C. D. Sloop and C. Liu (2012a), WWLLN
406 – ENTLN detection efficiency and the land ocean interface, *J. Geophys. Res*. (submitted).
407
408 Hutchins, M. L., R. H. Holzworth, J. B. Brundell, and C. J. Rodger (2012b), Relative detection efficiency
409 of the World Wide Lightning Location Network, *Radio Sci.* (submitted).
410
411 Jacobson, A. R., R. H. Holzworth, J. Harlin, R. L. Dowden, and E. H. Lay (2006), Performance
412 assessment of the World Wide Lightning Location Network (WWLLN), using the Los Alamos Sferic
413 Array (LASA) array as ground-truth, *J. Atmos. Oceanic Technol.*, 23, 1082–1092, doi:10.1175/
414 JTECH1902.1
415

Jayaratne E. R., C. P. R. Saunders, and J. Hallett (1983), Laboratory studies of the charging of soft hail during ice crystal interactions, *Q. J. R. Meteorol. Soc.*, 109, 609–630.

Kodama, H., Okabe, Y. Tomisaka, K. Kotono, Y. Kondo, and H. Kasuya (2007), Lightning frequency and microphysical properties of precipitating clouds over the western North Pacific during winter as derived from TRMM multisensor observations, *Mon. Wea. Rev.*, 135, 2226–2241.

Kummerow, C., W. Barnes, T. Kozu, J. Shiue, J. Simpson (1998), The Tropical Rainfall Measuring Mission (TRMM) sensor package, *J. Atmos. Oceanic Technol.*, 15, 809–817. doi: http://dx.doi.org/10.1175/1520-0426(1998)015<0809:TTRMMT>2.0.CO;2.

Lang, T. J., and S. A. Rutledge (2002), Relationships between convective storm kinematics, precipitation, and lightning, *Mon. Wea. Rev.*, 130, 2492-2506.

Latham, J., W. A. Petersen, W. Deierling, and H. J. Christian (2007), Field identification of a unique globally dominant mechanism of thunderstorm electrification, *Q. J. R. Meteorol. Soc.*, 133, 1453–1457.

Lay, E. H., R. H. Holzworth, C. J. Rodger, J. N. Thomas, O. Pinto Jr., and R. L. Dowden (2004), WWLL global lightning detection system: Regional validation study in Brazil, *Geophys. Res. Lett.*, 31, L03102, doi:10.1029/2003GL018882.

Liu, C., D. Cecil, and E. J. Zipser (2011), Relationships between lightning flash rates and passive microwave brightness temperatures at 85 and 37 GHz over the tropics and subtropics, *J. Geophys. Res.*, *116*, D23108, doi:10.1029/2011JD016463.

441 Mansell, E. R., D. R. MacGorman, C. L. Ziegler, and J. M. Straka (2005), Charge structure and lightning
442 sensitivity in a simulated multicell thunderstorm, *J. Geophys. Res.*, 110, D12101, DOI:
443 10.1029/2004JD005287.
444
445 Mohr, K., J. S. Famiglietti, and E. J. Zipser (1999), The contribution to tropical rainfall with respect to
446 convective system type, size, and intensity estimated from the 85-GHz ice-scattering signature, *J. Appl.*
447 *Meteor.*, 38**,** 596–605.
448
449 Nakamura, Y., et al. (2011), Global relationships between lightning and ice water path characteristics
450 from WWLLN and AMSU-B/MHS, *Fifth Conf. on Meteo. Applic. of Lightning Data*, Seattle, WA.
451 https://ams.confex.com/ams/91Annual/webprogram/Paper177798.html.
452
453 Nesbitt, S. W., E. J. Zipser, and D. J. Cecil (2000), A census of precipitation features in the tropics using
454 TRMM: Radar, ice scattering, and lightning observations, *J. Clim.*, 13, 4087–4106.
455
456 Nesbitt, S. W., and E. J. Zipser (2003), The diurnal cycle of rainfall and convective intensity according to
457 three years of TRMM measurements. *J. Clim.*, 16**,** 1456–1475.
458
459 Pessi, A., and S. Businger (2009), Relationships Between Lightning, Precipitation, and Hydrometeor
460 Characteristics over the North Pacific Ocean, *J. Appl. Meteor.*, 48, 833-848.
461
462 Petersen, W. A., H. J. Christian, and S. A. Rutledge (2005), TRMM observations of the global
463 relationship between ice water content and lightning, *Geophys. Res. Lett.*, 32, L14819,
464 doi:10.1029/2005GL023236.
465

Reynolds S. E., M. Brook, and M. F. Gourley (1957), Thunderstorm charge separation, *J. Meteorol.* 14, 163–178.

Rodger, C. J., J. B. Brundell, and R. L. Dowden (2005), Location accuracy of VLF World Wide Lightning Location (WWLL) network: Post-algorithm upgrade, *Ann. Geophys.*, 23, 277–290.

Rodger, C. J., S. Werner, J. B. Brundell, E. H. Lay, N. R. Thomson, R. H. Holzworth, and R. L. Dowden (2006), Detection efficiency of the VLF World-Wide Lightning Location Network (WWLLN): Initial case study, *Ann. Geophys.*, 24, 3197–3214.

Rodger, C. J., J. B. Brundell, R. H. Holzworth, and E. H. Lay (2009), Growing detection efficiency of the World Wide Lightning Location Network, *in Coupling of Thunderstorms and Lightning Discharges to Near-Earth Space: Proceedings of the Workshop,* edited by N. B. Crosby, T.-Y. Huang, and M. J. Rycroft, pp. 15–20, doi:10.1063/ 1.3137706, Am. Inst. of Phys., Melville, N. Y.

Solorzano, N. N., J. N. Thomas, and R. H. Holzworth (2011), Lightning flashes in 2005 - 2010 tropical cyclones: implications for intensity change and comparisons with convective and environmental parameters, *Fifth Conf. on Meteo. Applic. of Lightning Data*, Seattle, WA. https://ams.confex.com/ams/91Annual/webprogram/Paper185752.html

Takahashi, T. (1984), Thunderstorm electrification - A numerical study, *J. Atmos. Sci.*, 41, 2541-2558.

Toracinta, E. R., and E. J. Zipser (2001), Lightning and SSM/I-ice-scattering mesoscale convective systems in the global Tropics. *J. Appl. Meteor.*, 40**,** 983–1002.

Toracinta E. R., D. J. Cecil, and E. J. Zipser (2002), Radar, passive microwave, and lightning characteristics of precipitating systems in the Tropics, *Mon. Weather Rev.* 130, 802–824.

Vivekanandan, J., J. Turk, and V. N. Bringi (1991), Ice water path estimation and characterization using passive microwave radiometry. *J. Appl. Meteor.*, 30, 1407–1421.

Wiens, K. C., S. A. Rutledge, and S. A. Tessendorf (2005), The 29 June 2000 supercell observed during STEPS. Part II: Lightning and charge structure, *J. Atmos. Sci.*, 62, 4151–4177, doi:10.1175/JAS3615.1.

Wu, R., and J. A. Weinman (1984), Microwave radiances from precipitating clouds containing aspherical ice, combined chase, and liquid Hydrometeors, *J. Geophys. Res.*, *89*(D5), 7170–7178, doi:10.1029/JD089iD05p07170.

Xu, W. and E. J. Zipser (2012), Properties of deep convection in tropical continental, monsoon, and oceanic rainfall regimes, *Geophys. Res. Lett.*, *39*, L07802, doi:10.1029/2012GL051242.

Yan, B. and F. Weng (2009), Assessments of F16 Special Sensor Microwave Imager and Sounder antenna temperatures at lower atmospheric sounding channels, *Adv. Meteor.*, doi:10.1155/2009/420985

Zipser, E. J., D. J. Cecil, C. Liu, S. W. Nesbitt, and D. P. Yorty (2006), Where are the most intense thunderstorms on Earth?, *Bull. Amer. Meteorol. Soc.*, 87, 1057–1071.

Tables and Figures

Table 1: Satellite microwave radiometer data

Platform	Orbit	Instrument	Scanning Geometry	Frequencies (GHz) and Polarization	Resolution or Effective Field of View (km)	Swath Width (km)	Operational Period	Reference
TRMM	35° / 400 km	TMI	Conical	37 V/H, 85 V/H	7 × 5 at 85 GHz 16 × 9 at 37 GHz	759	1997-present	Kummerow et al., 1998
DMSP / F16	Polar / 830 km	SSMIS	Conical	91.7 V/H, 150 H, 183.3 ± 1, 3, 7 H	12.5 × 12.5	1707	2003-present	Yan and Weng , 2009

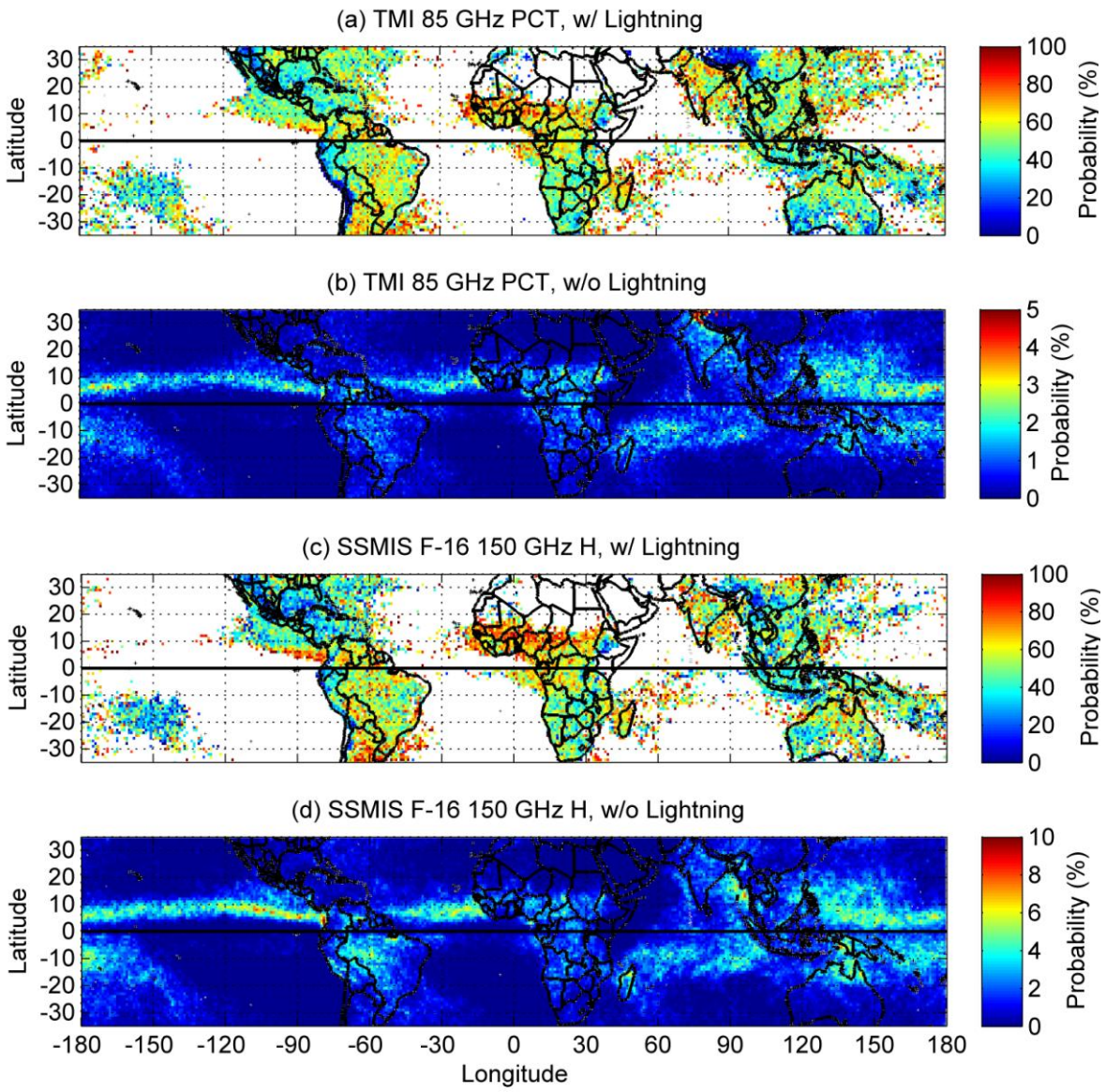

Figure 1: Probabilities of cold brightness temperatures (BTs) with and without lightning for warm seasons of 2009-2010 in the Northern Hemisphere (JAS) and 2010-2011 in the Southern Hemisphere (JFM). Percent of TMI 85 GHz PCT BTs below 195 K: (a) for at least two lightning counts and (b) no lightning in 0.5° × 0.5° mapping-bins. Percent of SSMIS/F16 150 GHz H BTs below 180 K: (a) for at least two lightning counts and (b) no lightning in 0.5°× 0.5° mapping-bins. Notable regions of convection include Central Africa, Madagascar, the Amazon Basin, the Congo Basin, Central America, Sub-Saharan Africa, India and Southeast Asia, East Pacific, and South Pacific Convergence Zone (SPCZ) as reported in Figure 1 of Mohr et al. [1999] and Figure 1 of Boccippio et al. [2000].

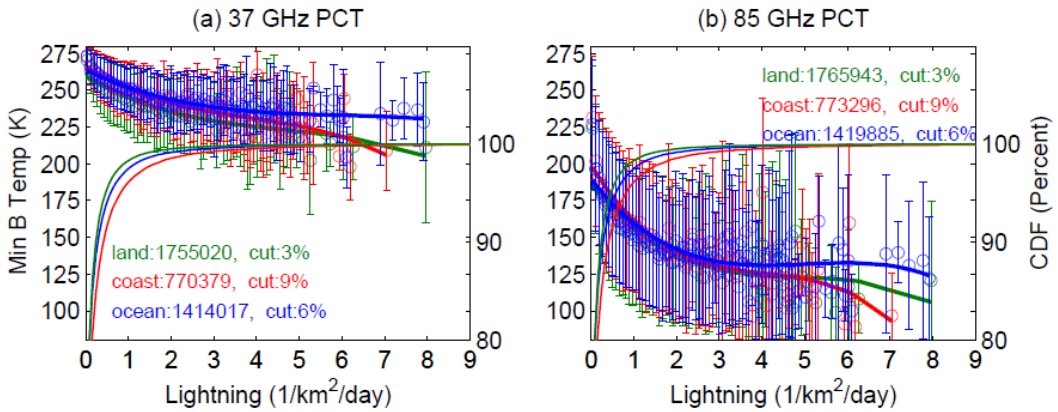

Figure 2: TMI 37 (a) and 85 (b) GHz PCT brightness temperatures (BTs) vs. WWLLN lightning rates for land (green), coast (red), and ocean (blue) regimes during warm seasons of 2009-2010 in the Northern Hemisphere (JAS) and 2010-2011 in the Southern Hemisphere (JFM). Lightning counts and minimum BTs are found in 0.5°×0.5° mapping-bins. Lightning occurred within +/- 15 min. of the BT observations. Circles are the averages of the minimum BT within the lightning-bins, and the error bars are the standard deviations of the BTs. Cubic least-squares fits to the average BTs are shown as thick lines, and cumulative distribution functions (CDFs) of the lightning rate samples are shown on the right ordinate as thinner lines.

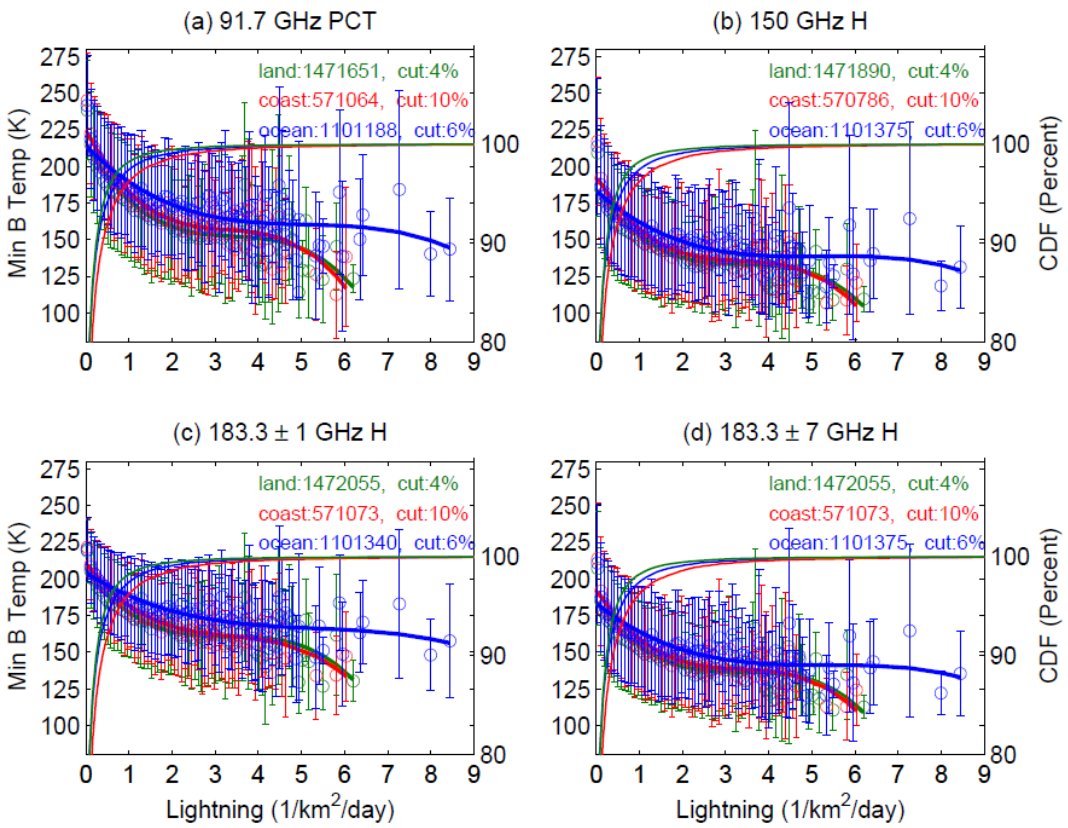

Figure 3: SSMIS/F16 91 GHz PCT (a), 150 (b), 183.3 ±1 (c), and 183.3 ±7 GHz H vs. WWLLN lightning rates. Data are from the warm seasons of 2009-2010 in the Northern Hemisphere (JAS) and 2010-2011 in the Southern Hemisphere (JFM). See Figure 2 caption for details.

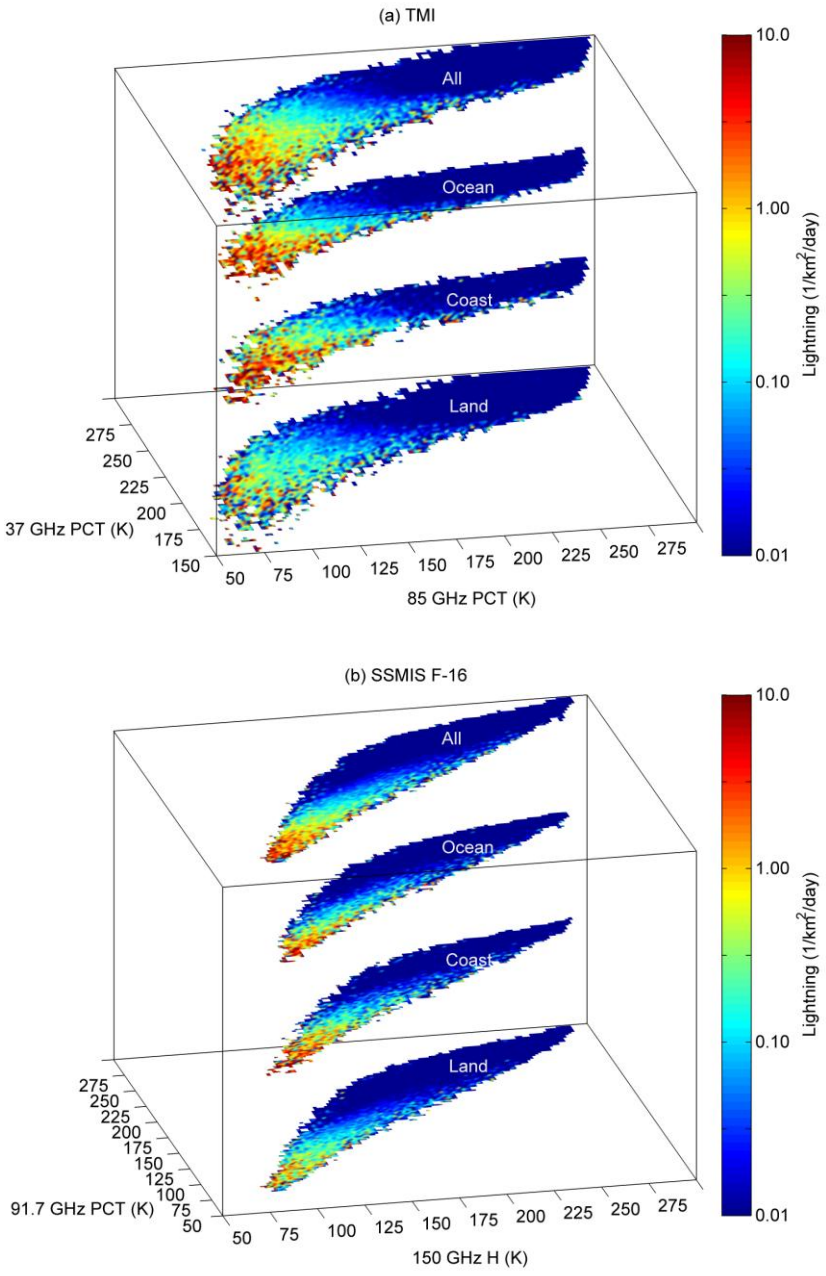

Figure 4: Scatter plots of (a) TMI 37 and 85 GHz PCT and (b) SSMIS/F16 91 GHz PCT and 150 GHz H along with mean WWLLN lightning rates. Data are from the warm seasons of 2009-2010 in the Northern Hemisphere (JAS) and 2010-2011 in the Southern Hemisphere (JFM). Lightning counts and minimum BTs are found in 0.5°×0.5° mapping-bins. Lightning occurred within +/- 15 min. of the BT observations.